Zeolite Y supported nickel phosphide catalysts for the hydrodenitrogenation of quinoline as a proxy for crude bio-oils from hydrothermal liquefaction of microalgae

Jonathan L. Wagner,[a,b] Emyr Jones, [c] Asel Sartbaeva,[c] Sean A. Davis,[d] Laura Torrente-Murciano,[e] Christopher J. Chuck[b] Valeska P. Ting[f*]

[a] *Centre for Doctoral Training in Sustainable Chemical Technologies, University of Bath, Claverton Down, Bath, United Kingdom, BA2 7AY.*

[b] *Department of Chemical Engineering, University of Bath, Claverton Down, Bath, United Kingdom, BA2 7AY.*

[c] *Department of Chemistry, University of Bath, Claverton Down, Bath, United Kingdom, BA2 7AY.*

[d] *School of Chemistry, University of Bristol, Bristol BS8 1TR, UK*

[e] *Department of Chemical Engineering, University of Cambridge, Pembroke Street, CB2 3RA, UK*

[f] *Department of Mechanical Engineering, University of Bristol, Bristol BS8 1TR, UK*

[*] *v.ting@bristol.ac.uk*

Abstract

This work demonstrates the potential of zeolite Y supported nickel phosphide materials as highly active catalysts for the upgrading of bio-oil as improved alternative to noble metal and transition metal sulphide systems. Our systematic work studied the effect of using different counterions (NH_4^+, H^+, K^+ and Na^+) and Si/Al ratios (2.56 and 15) of the zeolite Y. It demonstrates that whilst the zeolite counterion itself has little impact on the catalytic activity of the bare Y-zeolite, it has a strong influence on the activity of the resulting nickel phosphide catalysts. This effect is related to the nature of the nickel phases formed during the synthesis process Zeolites containing K^+ and Na^+ favour the formation of a mixed $Ni_{12}P_5/Ni_2P$ phase, H^+ Y produces both Ni_2P and metallic Ni, whereas NH_4^+ Y produces pure Ni_2P, which can be attributed to the strength of the phosphorus-aluminium interaction and the metal reduction temperature. Using quinoline as a model for the nitrogen-containing compounds in bio-oils, it is shown that the hydrodenitrogenation activity increases in the order $Ni_2P > Ni^0 > Ni_{12}P_5$. While significant research has been dedicated to the development

of bio-oils produced by thermal liquefaction of biomass, surprisingly little work has been conducted on the subsequent catalytic upgrading of these oils to reduce their heteroatom content and enable processing in conventional petrochemical refineries. This work provides important insights for the design and deployment of novel active transition metal catalysts to enable the incorporation of bio-oils into refineries.

1   Introduction

Recent developments in the thermal liquefaction of biomass have demonstrated the feasibility of producing bio-oils from a range of terrestrial and marine biomass feedstocks on both pilot and industrial scale. [1] Compared to crude fossil oils, the bio-oils produced contain much higher concentrations of oxygen, typically between $5 - 15$ wt.% for oils produced via hydrothermal liquefaction (HTL), or up to 40 wt.% in the case of pyrolysis oils. [2-4] Bio-oils tend to contain lower sulphur concentrations than crude oil, in general less than 1 %. In addition, the processing of protein-rich biomass, such as microalgae, can lead to nitrogen contents exceeding 8 wt.%, normally present as low molecular weight heterocycles [4, 5]. However, the high oxygen and nitrogen content of these bio-oils restricts their direct processing within conventional petrochemical refineries. [6, 7] Consequently, significant pre-treatment is required to reduce the biocrude heteroatom content, particularly nitrogen, to an acceptable level (< 0.25 %). [8, 9]

Despite this, relatively little research has been conducted on the denitrogenation of components present in bio-oils. [10-12] Most existing studies have been conducted under batch conditions using either noble metal (Pt, Pd, Ru, Rh) [12-19] or transition metal sulphide catalysts (CoMo, NiMo) [14, 19-21]. Whilst noble metal catalysts are expensive, transition metal sulphide catalysts require the presence of sulphur to retain their activity. Therefore, these sulphide catalysts may be unsuitable for the conversion bio-oils, which contain only trace amounts of sulphur. This explains the negligible or minor activity for the reduction of the nitrogen and oxygen content of the bio-oil observed in many studies, whilst increasing the formation of coke and gaseous by-products. [12, 17]

An alternative class of hydrotreating catalysts are the transition metal phosphides, which include Ni_2P and MoP, which have been shown to possess significantly higher denitrogenation activities than commercial bimetallic transition metal sulphides. [22-25] Their high activities have been related to isotropic external morphologies, compared to the layered structure in sulphides, exposing a greater number of coordinatively unsaturated surface atoms and improving their dispersion when supported on high surface area materials. [26-28] As transition metal phosphides are stable in the absence of sulphur containing compounds, [25, 29, 30] they could be particularly suitable for the conversion of nitrogen-rich sulphur-low bio-oils. [31, 32]

Most transition metal phosphides have been either supported on silica [33, 34] or used in the bulk phase, [35-37] but increasingly, alternative supports such as alumina, [38] MCM-41 [25, 39] and zeolites [27, 40] are being studied. One of the advantages of using zeolites as catalyst supports is their regular and tuneable pore structure, which promotes shape-selective catalysis. Furthermore, aluminium-containing zeolite supports possess additional acid sites, which may help to protonate the nitrogen group, facilitating the cleavage of the aliphatic C-N bonds via E_2 elimination reactions. [41, 42] The acid sites may also catalyse cracking reactions to break large polyaromatic compounds into lighter oil fractions, [40] thereby helping to reduce the bio-oil viscosity. However, the formation of active transition metal phosphide catalysts on aluminium-containing supports is hindered by the formation of $AlPO_4$ during the calcination of the catalyst precursors. [43] Because of this, the formation of the desired Ni_2P phase requires a large excess of phosphorus [39, 44] and much higher reduction temperatures [45, 46] to form the desired Ni_2P phosphide phase. This can result in increased particle agglomeration, reducing the metal dispersion on the catalysts, whilst also having adverse effects on the structure of the support. [46] A potential way of modifying the interaction between phosphorus and the support is to use zeolites with different counterions as found during the synthesis of Rh phosphide catalysts supported on MFI zeolites.[45] Catalysts supported on Na^+ MFI required much lower reduction temperatures, allowing the formation of smaller nanoparticles, than their H^+ MFI counterparts.

Another challenge for the design of such catalysts for bio-oil upgrading is that mass transfer limitations within microporous zeolite pores may restrict reactions to the outer zeolite surface, particularly for the larger molecules found within most bio-oils, reducing overall reaction rates. Consequently, attempts have been made to synthesize zeolites with hierarchical pore dimensions containing additional mesopores within the zeolite framework.

[47] These modifications can be achieved either during the zeolite synthesis itself through the use of templates, or using post synthetic modification methods such as steam processing or chemical modification. [48] One promising approach for introducing mesoporosity to zeolites to increase mass transport is through base leaching with NaOH. This leaching results in partial dissolution of the zeolite crystal [49], allowing the external surface area and mesopore volume of the resulting material to be controlled via the NaOH concentrations and exposure period.

Within this context, the objective of this current study was to develop novel nickel phosphide catalysts supported on zeolite Y as a novel alternative to noble metal and transition metal sulphide catalysts for the upgrading of bio-oils. As crude bio-oils consist of a highly complex mixture of molecules, with complex analytical challenges, a model compound (quinoline) was used as a proxy for the cyclic nitrogen compounds present in crude bio-oils. (In fact, bio-oils also contain a range of other nitrogen compounds such as amines and amides, but these are expected to be more easily upgraded). ,In order to investigate the effect of the zeolite support on the formation of the active Ni_2P phase and overall catalytic activity, a range of zeolite supports were tested containing different counterions and silicon-to-aluminium (Si/Al) ratios. To investigate the use of base leaching to improve mass-transfer characteristics of these zeolite supports, selected zeolites were exposed to base treatment prior to catalyst impregnation, to investigate the potential of introducing additional mesoporosity into the zeolite structure and subsequent effects on the catalytic activity of the materials.

2 Experimental procedure

2.1 Catalyst synthesis

Commercial Na^+ Y and NH_4^+ Y zeolites (Molecular sieves, powder, Si/Al ratio: 2.56) were obtained from Sigma-Aldrich while H^+ Y_L zeolite (SiO_2/Al_2O_3 mol ratio: 30:1, powder form) was obtained from Alfa Aesar. H^+ Y zeolite was obtained by calcination of the commercial NH_4^+ Y zeolite in static air at 550 °C for 5 h. Ni^{2+} Y and K^+ Y zeolites were prepared by single-stage ion exchange of the commercial Na^+ Y zeolite with solutions of nickel nitrate ($Ni(NO_3)_2 \cdot 6H_2O$) and potassium nitrate (KNO_3), respectively, using a 2:1 excess of the counter-ion to be exchanged. The exchange solutions were stirred for 6 h at 600 rpm at room temperature, followed by centrifugation and washing of the exchanged zeolite with deionized water.

Base-treatment of the commercial NH_4^+ Y zeolite was conducted by combining 50 mL of a 0.625 M NaOH solution with 50 mL of an aqueous TPABr solution of 0.05 M (equivalent to 0.2 g g^{-1}, for mild treatment, MT) or 0.24 M (0.92 g g^{-1}, for harsh treatment, HT). After mixing for 30 minutes, 3.3 g of zeolite was added to the solution and the suspension was stirred for further 30 minutes at a temperature of 65 °C. The product was filtered and dried at 65 °C in a preheated oven for 24 h.

Nickel phosphide supported catalysts were prepared by incipient wetness impregnation of the zeolites with nickel nitrate hexahydrate ($Ni(NO_3)_2.6H_2O$) and ammonium phosphate, (($NH_4)_2HPO_4$) solutions, to obtain a nominal nickel loading of 5 wt.% and P/Ni ratios of 3.0. Two methods of impregnation were investigated. The impregnation was either conducted in two stages (first impregnation with nickel nitrate, followed by drying at 120 °C and impregnation with ammonium phosphate) [36, 40] or in a single-stage by dissolving the two salts together in a 2.5 M nitric acid solution before impregnation on the support. [24, 50]

The impregnated materials were dried overnight at 120 °C, calcined at 400 °C for 4 hours and pre-reduced for 4 hours at 550 °C under 120 mL min^{-1} hydrogen flow. Subsequently, the materials were allowed to cool before passivation by flowing 250 mL min^{-1} of 1 % O_2/N_2 for 4 hours.

2.2 Catalyst characterization

Power X-Ray diffraction data was collected on a BRUKER D8 Advance diffractometer with a Cu Kα X-ray source (λ = 1.54 Å). The cell parameters were determined using the *Unit Cell* least squares refinement program, [51] and the simulated XRD powder pattern for cubic faujasite was used to index the peaks. [52] The Scherrer crystallite size was calculated using the full width at half maximum (FWHM) of the strongest metal peaks, corresponding to the dominant Ni phase ([2 -1 1], [2 0 1] and [3 -1 0] for Ni_2P; [1 1 1], [2 0 0] and [2 2 0] for Ni and [1 1 2], [4 0 0] and [3 1 2] for $Ni_{12}P_5$). The surface areas of the different materials were determined by nitrogen adsorption at 77 K after degassing at 300 °C for 12h on a Micromeritics 3Flex analyser using the Brunauer-Emmett-Teller (BET) method and applying the Rouqerol consistency criterion for microporous samples.

SEM-EDX analyses were conducted on a JEOL IT-300 Scanning Electron Microscope fitted with an Oxford instruments Aztec X-Max^N 80 T EDX detector. EDX spectra were collected using area scans at a magnification of 1000X, an acquisition time of 150 s and an accelerating voltage of 20 keV. For each sample, at least three scans of separate areas were conducted,

normalized to exclude carbon and averaged to determine the Ni loading, Ni/P ratios, Si/Al ratios and the counter-ion to aluminium ratios. STEM-EDX analyses were conducted on a JEM-2100F Field Emission Transmission Electron Microscope using a JEOL high-angle annular dark-field (HAADF) STEM detector and corresponding elemental maps were collected, using a minimum of 20 frame counts for each analysis using the Aztec X-MaxN 80 T detector. Particle sizes were determined from STEM images using the ImageJ open source image processing software using the oval shape selector tool to manually outline each particle to the maximum diameter.

2.3 Hydrodenitrogenation reaction of quinoline

Hydrodenitrogenation reactions were conducted in 6 mL stainless steel batch reactors, connected to a pressure gauge, vent valve and fitted with an internal thermocouple. The reactors were heated inside a Micromeritics FlowPrep 060 furnace set at 400 °C. The total reaction time for each experiment was 2 hours, after which the reactors were left to cool in ambient air. In a typical reaction, 50 mg of catalyst dispersed in 1 g of silica gel was added to 1 mL 10 vol.% (14.1 wt%) quinoline in dodecane solution. The sealed reactors were purged with nitrogen and pressurised with hydrogen to 40 bar. Reactions were conducted in triplicate to determine the standard deviation. Reaction products were analysed by ^{1}H NMR and ^{13}C NMR obtained on a 400 MHz Bruker AVANCE III spectrometer and GC-MS analysis obtained on an Agilent 7890B Gas Chromatograph (DB-FFAP column, 30 m, 0.25 mm x 0.25 μm). For the GC-MS analysis, the samples were dissolved in toluene with an injection volume of 1 μL. Samples were loaded at 40 °C, with a hold time of 1 min, followed by ramping at 10 °C min^{-1} to 60 °C, hold time of 4 min, and ramping at 10 °C min^{-1} to 250 °C, with a hold time of 4 min. The MS detector was turned off between 3.60 min and 5.50 min.

The conversion of quinoline and the yields of the 1,2,3,4-tetrahydroquinoline (1234THQ), 5,6,7,8-tetrahydroquionoline (5678THQ) and orthopropylaniline (OPA) breakdown products were calculated using the GC-MS data and verified against the ^{1}H NMR data from the same materials. Conversion/product yields were calculated from the compound to dodecane peak ratios, using standard calibration curves:

Conversion = 1- $(A_Q/A_{C12})_{product}/(A_Q/A_{C12})_{initial}$

Yield = $m_P/m_{Q,feed}$

Where A_Q and A_{C12} represent the peak areas of quinoline and dodecane, respectively, whilst the mass of product, m_P, was calculated from the calibration curve.

The remaining reaction products, including decahydroquinoline (DHQ), propylbenzene (PB), propylcyclohexylamine (PCHA) and propylcylcohexane (PCH) could not be quantified by either analysis method, due to overlap with the solvent and other product peaks, and consequently were grouped together as 'other' and calculated by difference:

$$Yield(Other) = Conversion(Quinoline) - Yield(1234THQ) - Yield(5678THQ) - Yield(OPA)$$

3 Results and discussion

Bio-crudes formed by hydrothermal liquefaction of microalgae generally consist of a highly complex mixture of molecules, including lipid derived alkanes and alkenes, nitrogen containing compounds such as amines and amides, oxygen containing compounds such as alcohols, aldehydes and ketones, and heterocyclics such as furans, indoles or pyrroles. [53] In order to simplify the analytic challenge associated to complex mixtures and to provide mechanistic understanding, we use quinoline as a model heterocycle, allowing the evaluation of the three major reaction pathways associated for the denitrogenation reaction (Figure 1): *i.* hydrogenation of the nitrogen ring, to convert aromatic carbon-nitrogen bonds into single, aliphatic bonds; *ii.* sequential hydrogenolysis of the C-N bonds *iii.* saturation of the aromatic ring adjacent to the nitrogen heterocycle. [54, 55] However, it should be noted that additional cracking reactions may be required to facilitate the conversion of heavily substituted nitrogen rings, as found during the conversion of heavier, synthetic crude oils. [56] The removal of nitrogen from heterocyclic compounds is intrinsically more difficult than from less strongly bound compounds or removal of other heteroatoms. Therefore, quinoline was chosen to represent the most challenging target. A catalyst that is active in the upgrading of quinoline is also expected to be active for the upgrading of the other components in bio-oil.
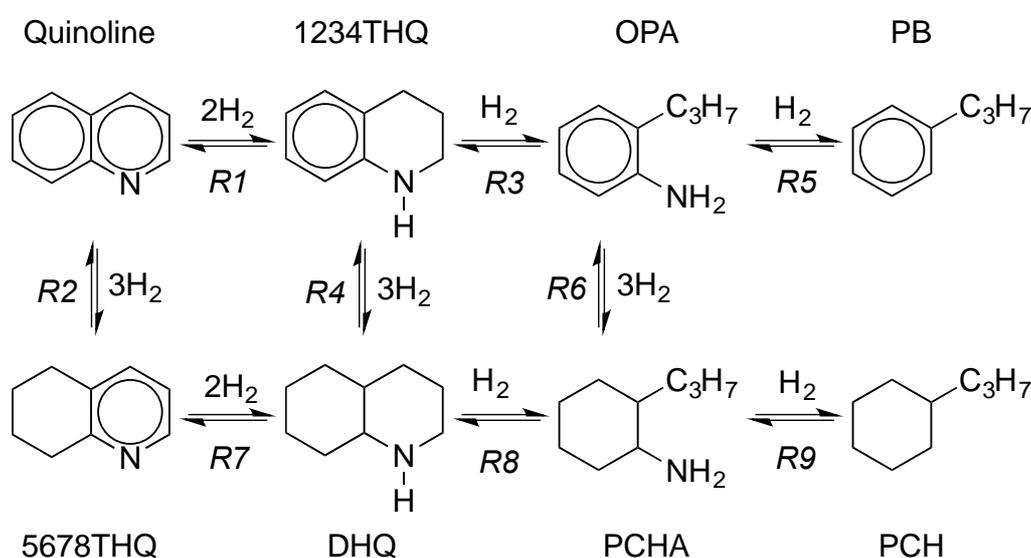
Figure 1: Pathway for the hydrodenitrogenation of quinoline

3.1   Effect of zeolite counter-ion

A first series of experiments was conducted to study the effect of the number (Si/Al ratios of 2.7 and 15) and choice (NH_4^+, H^+, Na^+ and K^+) of the zeolite counter-ions on the formation and activity of zeolite Y supported nickel phosphide catalysts for the conversion of quinoline. To investigate the contribution of the zeolite support itself to the overall catalytic activity, the conversions of quinoline and the resulting product distributions were first investigated over the bare zeolites Y and compared to an uncatalysed (blank) reaction under the same conditions. Subsequently, the various zeolites were used as supports for the nickel phosphide catalysts, and their relative quinoline conversion activities were correlated to differences in their active phases.

3.1.1   Conversion over bare zeolites

In the absence of any catalyst, the quinoline conversion at 400 °C reached 24 %, producing a mixture 1234THQ (9 %) and other unidentified products (Figure 2). As expected, the addition of bare, untreated Y-zeolite catalysts resulted in an increase of the overall quinoline conversion, but the yields of 1234THQ remained either equal or lower compared to the blank reaction. The increase in conversion and reduction in 1234THQ yields in the presence of these zeolites is believed to be the result of increased cracking reactions over the zeolitic acid sites, increasing the amount of side products not directly associated with the quinoline denitrogenation pathway, such as indoline, isoquinoline, *o*-toluidine, *o*-phenylpropylamine, aniline, toluene and *o*-ethylaniline, as previously reported. [57] In all cases, the presence of the bare zeolites appears to have minimal impact on the formation of 1234THQ compared to the blank reaction and this suggests that the zeolites display little activity for the initial hydrogenation step. It is possible that for both the blank reaction and the reactions over the bare zeolites the formation of 1234THQ is catalysed by stainless steel reactor instead, which contains a number of potentially active materials such as nickel, molybdenum or chromium.

The increase in quinoline conversion appears to be independent of the physical properties of the different NH_4^+ Y, H^+ Y, Na^+ Y, K^+ Y and H^+ Y_L zeolites such as the BET surface area or the cell parameter (Table 1). Indeed, the two highest quinoline conversions were obtained over the H^+ Y and H^+ Y_L zeolites, which have very different Si/Al ratios, surface areas and cell parameters. Instead, the differences in activities are likely to be related to the differences in the number of acid sites. H^+ Y is known to possess a higher Brønsted acidicty than the Na^+

or K^+ forms, [27, 45] whereas NH_4^+ Y is expected to transform to the H^+ form under reaction conditions, explaining the trend in the conversion activity: $H^+ > NH_4^+ > K^+ > Na^+$. Similarly, as a result of its higher Si/Al ratio, H_L^+ Y contains significantly fewer Brønsted acid sites than H^+ Y and consequently its activity is significantly reduced.

All zeolites displayed characteristic zeolite Y XRD diffraction patterns (supplementary information) with cell parameters ranging from 24.23 Å for H^+ Y_L to 24.61 Å for NH_4^+ Y. The differences in cell parameters can generally be attributed to the counterion size (bigger K^+ and NH_4^+ ions form larger cell parameters than Na^+ or H^+) and the Si/Al ratio (lower Al content reduces the counterion concentration). For the same reasons, the BET surface areas decrease from 919 m^2 g^{-1} ±1.4 m^2 g^{-1} for H^+ Y_L, to 765 m^2 g^{-1} ±1.0 m^2 g^{-1} for NH_4^+ Y, as the larger counterions decrease the internal pore volume and surface area.
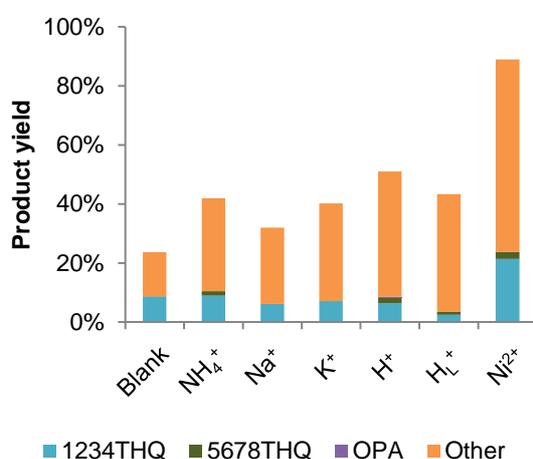

Figure 2: Quinoline conversion and product distribution over bare Y-zeolites containing different counterions at 400 °C.

To investigate the effect of introducing nickel into the zeolite structure itself, Ni^{2+} Y zeolite was synthesised by single-step ion exchange of Na^+ Y with a nickel nitrate solution. Whilst the other counterions (NH_4^+, H^+, Na^+ and K^+) showed a similar quinoline conversion to the bare zeolites Y, a considerably higher conversion of 89 % was achieved over the Ni^{2+} Y zeolite. In addition, the 1234THQ yield was increased to 21.3 %, together with the formation of small amounts of 5678THQ (2.4 %), but their values remain relatively low with respect to the unaccounted 'other' product fraction.

The presence of 5678THQ suggests that both the hydrogenation of the first and second aromatic rings are feasible in the presence of Ni^{2+}, although the hydrogenation of the nitrogen containing ring is favoured as shown by the high 1234THQ to 5678THQ yield ratio. Further analysis of the products over the Ni^{2+} Y zeolite by ^{13}C NMR confirms the formation of

1234THQ and 56789THQ and the small presence of fully hydrodenitrogenated product PCH and the reaction intermediate OPA (supplementary information). Consequently divalent nickel ions appear to possess intrinsic hydrogenation activity when integrated within the zeolite framework, potentially by combining Lewis acidity and aiding the absorption of basic quinoline molecules with its high hydrogenation activity.[58]

Table 1: Properties of different Y-zeolite materials.

Zeolite	Si/Al ratio (from SEM-EDX)	Molar ratios w.r.t. Al				BET Surface area / $m^2\ g^{-1}$	a / Å
		Na^+	K^+	Ni^{2+}	NH_4^+		
Untreated zeolites							
NH_4^+ Y	2.51*	0.19*	-	-	1.29[+]	764	24.61
Na^+ Y	2.7	0.90	-	-	-	888	24.24
K^+ Y	2.6	0.24	0.77	-	-	780	24.55
H^+ Y	2.5	0.19	-	-	-	843	24.47
H^+ Y_L	17.9	0.02	-	-	-	919	24.23
Ni^{2+} Y	2.5	0.46	-	0.32	-	802	24.60
Base treated zeolites							
NH_4^+ Y-MT	2.6	1.07	-	-	-	897	24.52
NH_4^+ Y-HT	2.5	1.07	-	-	-	855	24.53
H^+ Y_L-MT	12.2	0.73	-	-	-	684	24.33
H^+ Y_L-HT	11.5	1.23	-	-	-	716	24.22

Assumed equal to H^+ Y, [+]Based on supplier information

3.1.2 Conversion over Ni-P catalysts

As described in the experimental section (section 2.1) the zeolite Y supported nickel phosphide catalysts were prepared by two different methods of impregnation: *i.* two-stage impregnation where the zeolite was first impregnated with the nickel precursor (nickel nitrate) followed by drying and subsequent impregnation with ammonium phosphate and *ii.* single-stage impregnation with an acidified nickel phosphate solution. These two methods represent the most commonly used techniques used in the literature. Whilst single stage impregnation is expected to yield a more uniform catalyst distribution with a constant Ni/P ratio, the high acidity of the impregnation solution could have a detrimental effect on the support. Furthermore, initial impregnation with the nickel precursor may result in shielding

of the aluminium sites on the support, resulting in reduced interaction with phosphorus during the subsequent impregnation step.

All the resulting catalysts provided high quinoline conversion activities, ranging from 72 % with Ni_xP_y/K^+ Y (two-stage impregnation) to 94 % over Ni_xP_y/NH_4^+ Y catalyst (two-stage impregnation) (Figure 3).

In contrast to the activities of the bare Y zeolites, the quinoline conversions and product distributions achieved over the nickel phosphide catalysts were clearly dependent on the counterion in the zeolite Y support. This could be attributed to the effect of the counterion on the formation of the active phosphide phase, as previously observed in the literature. [45] Interestingly, the method of impregnation (two-stage or single-stage impregnation) had a limited impact on the product distributions obtained over the Ni_xP_y/Na^+ Y and Ni_xP_y/K^+ Y catalysts, whereas the product distributions over the Ni_xP_y/NH_4^+ Y and Ni_xP_y/H^+ Y catalysts were considerably different for the two synthesis methods. In all cases, the two-stage impregnation resulted in a significantly higher loss of surface area and zeolite crystallinity (indicated by an increased FWHM of the [1 1 1] diffraction peak) for all four catalysts (Table 2). This could be due to the formation of nickel phosphate precipitates on the zeolite surface, blocking the zeolite pores and preventing the escape of moisture and reaction gases during the subsequent reduction process, resulting in the build-up of internal pressure and ultimately leading to structural loss. The effect is particularly pronounced in the NH_4^+ Y zeolite, as the thermal decomposition of ammonium ions releases significant quantities of ammonia in addition to the other reaction gases.

It is notable that the reactions over the NH_4^+ Y, H^+ Y and Na^+ Y zeolites all yielded similar amounts of the undetermined 'other' product phase, whereas the yield over the K^+ Y catalyst was much lower. A potential explanation is the very low Brønsted acidity of these catalysts, eliminating the occurrence of cracking reactions, demonstrated during the conversion of tridecane over Ni_2P catalysts supported over HUSY and KUSY zeolites. [27]
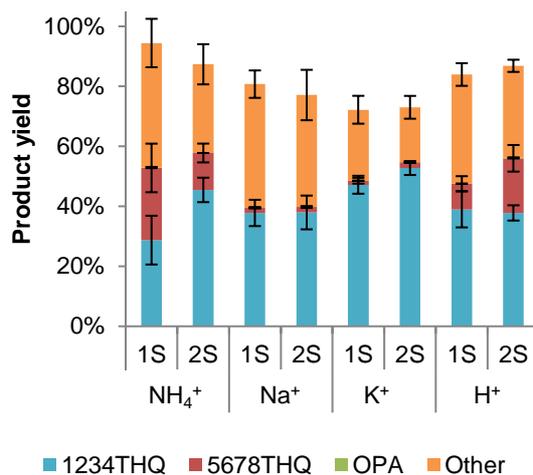
Figure 3: Quinoline conversion over nickel phosphide catalysts supported on zeolites Y containing different counterions prepared by two-step (2S) and single-step (1S) impregnation methods

Further characterisation of these materials by XRD provides insights about the active nickel sites present in the catalysts (Figure 4). K^+ Y and Na^+ Y zeolite-supported catalysts display a mixture of $Ni_2P/Ni_{12}P_5$ phases for both methods of impregnation; H^+ Y zeolite supported catalysts show a pure Ni_2P phase for two-stage impregnation, in addition to metallic Ni for single stage impregnation; whilst NH_4^+ Y zeolite supported catalysts displayed Ni_2P peaks for both methods of impregnation together with small quantities of metallic nickel in the two-step impregnation catalyst. The improved formation of Ni_2P supported on H^+ Y zeolite during two-step impregnation could be related to the reduced interaction between phosphorus and the support due to the shielding of aluminium sites with the nickel precursor. In contrast, the interaction between aluminium and phosphorus is weaker for the zeolites containing the other three counterions, and consequently the method of impregnation has a lesser impact. The exception is the catalysts supported on NH_4^+ Y, where the extensive structural collapse during two-step impregnation could trap nickel particles, preventing their subsequent reaction with phosphorus.   The Scherrer equation was used to estimate the crystallite particle sizes of the different nickel species (Table 2). K^+ Y and Na^+ Y zeolite nickel-supported catalysts show Ni_2P particles ranging from ~ 36 nm to ~ 44 nm in addition to similarly-sized $Ni_{12}P_5$. In contrast, the H^+ Y and NH_4^+ Y zeolite-supported catalysts contain significantly smaller Ni_2P particles, particularly for single-step impregnation, with sizes ranging from 18 to 33 nm.
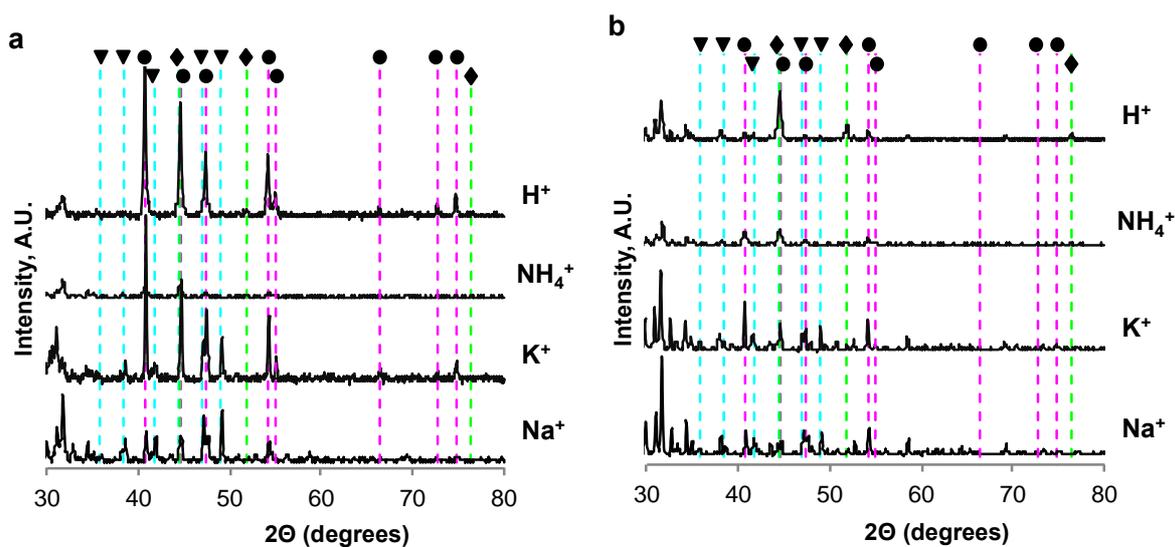
Figure 3: Powder XRD spectra of nickel phosphide catalysts supported on zeolites Y with different counterions prepared by (a) two-step impregnation, (b) single-step impregnation. (◆ = Ni^0, ● = Ni$_2$P, ▼ = Ni$_{12}$P$_5$)

Clear trends can be extracted from these data. Catalysts containing the Ni$_{12}$P$_5$ phase (Ni$_x$P$_y$/Na$^+$ Y and Ni$_x$P$_y$/K$^+$ Y) display a lower overall activity for the conversion of quinoline and yield negligible amounts of 5678THQ compared to the rest of the catalysts, suggesting that the Ni$_{12}$P$_5$ phase is less active than Ni$_2$P and metallic Ni. [60] In addition, the presence of the metallic Ni phase in Ni$_x$P$_y$/NH$_4^+$ Y (two-step impregnation) and Ni$_x$P$_y$/H$^+$ Y (single-stage impregnation) seems to be directly related to a decrease of the 5678THQ yield, while similar overall conversions are achieved with respect to their counterpart catalysts where only Ni$_2$P is present. This observation suggests that metallic Ni mainly favours the hydrodenitrogenation route initiated by the hydrogenation of the nitrogen-containing aromatic ring to form 1234THQ as the first intermediate product. In contrast to this, Ni$_2$P allows both the hydrogenation of the nitrogen-containing aromatic ring *and* the saturation of the aromatic rings adjacent to the nitrogen heterocycle as the initial reaction step, leading to a higher final yield of fully hydrodenitrogenated reaction products. [60] It is likely that the high overall activity and 5678THQ selectivity of the Ni$_x$P$_y$/NH$_4^+$ Y zeolite catalyst prepared by single-stage impregnation is also related to the smaller Ni$_2$P crystallite size (18 nm), compared to the other zeolite Y supported catalysts. This would be consistent with previous studies in the literature that have identified two different types of catalytic sites for Ni$_2$P: tetrahedral sites, which are more predominant in the bulk phase, and square pyramidal sites, more predominant in smaller nanoparticles, and more active towards hydrogenation reactions. [61]

13

Table 2: Physical properties of nickel phosphide catalysts supported on zeolite Y with different counterions

Support	SEM-EDX analysis		BET Surface area / $m^2\ g^{-1}$	FWHM of [1 1 1] zeolite peak, degrees	Ni phase	Ni-P particle size / nm
	Ni loading / % wt.	*Ni/P ratio*				
Two-step impregnation						
NH_4^+ Y	*nd*	*nd*	7.9	0.836	Ni_2P/Ni	26.53^+
Na^+ Y	*nd*	*nd*	214	0.246	$Ni_2P/Ni_{12}P_5$	41.27^* 38.72^+
K^+ Y	*nd*	*nd*	22	0.443	$Ni_2P/Ni_{12}P_5$	43.34^+
H^+ Y	5.8	0.58	92	0.492	Ni_2P	33.19^+
Single-step impregnation						
NH_4^+ Y	2.6^x	0.23^x	226	0.246	Ni_2P	18.08^+
Na^+ Y	5.5	0.58	322	0.197	$Ni_2P/Ni_{12}P_5$	35.81^* 36.73^+
H^+ Y	4.3	0.48	314	0.246	Ni_2P/Ni	26.70^i
K^+ Y	3.9	0.55	265	0.197	$Ni_2P/Ni_{12}P_5$	44.10^+

$Ni_{12}P_5$, $^+Ni_2P$, ^{i}metallic Ni, ^{x}calculated from STEM-EDX analysis

STEM characterisation of the Ni_xP_y/NH_4^+ Y catalysts prepared by single-stage impregnation shows that the average particle size measured from the TEM images (~ 20 - 25 nm) is in good agreement with that calculated by X-ray diffraction (Figure 5). In contrast, the TEM images for Ni_xP_y/H^+ Y display nickel-based particles with sizes ~ 60 nm, which might be formed by small aggregation of crystallites with sizes of 25-30 nm (Figure 6).

Elemental mapping by STEM-EDX of both materials also confirmed that nickel was mostly confined to the nanoparticles, whereas phosphorous was evenly distributed over the entire surface of the zeolite, with a slightly increased concentration on the nickel-rich nanoparticles. This observation confirms the strong interaction of phosphorus with the zeolite structure itself, [43] but makes it difficult to accurately determine the Ni/P ratio of the catalytic nanoparticles, and consequently its effect on the resulting catalytic hydrodenitrogenation activity of the material. Nonetheless, all materials experienced a significant increase in the overall Ni/P ratio during the synthesis process, which can be attributed to the release of phosphine gas (PH_3) during the reduction step. [34] It is also noticeable that for the catalysts prepared by single-step impregnation the highest Ni/P ratios were observed over those

supported on the K^+ Y and Na^+ Y zeolites, which displayed the Ni-rich $Ni_{12}P_5$ phase in addition to the Ni_2P phase. This suggests that the formation of Ni_2P over these materials was P-limited, and could indicate a much weaker interaction between phosphorus and the support, resulting in extensive P loss prior to sufficient reduction of the metal phase.
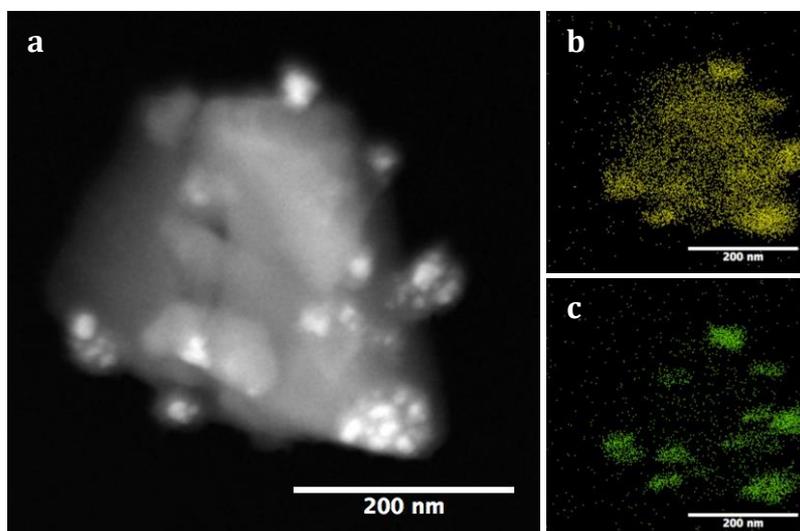

Figure 4: Elemental mapping by TEM of Ni_xP_y/NH_4^+ Y zeolite catalyst prepared in a single-step impregnation (a) Electron image, (b) P distribution, (c) Ni distribution
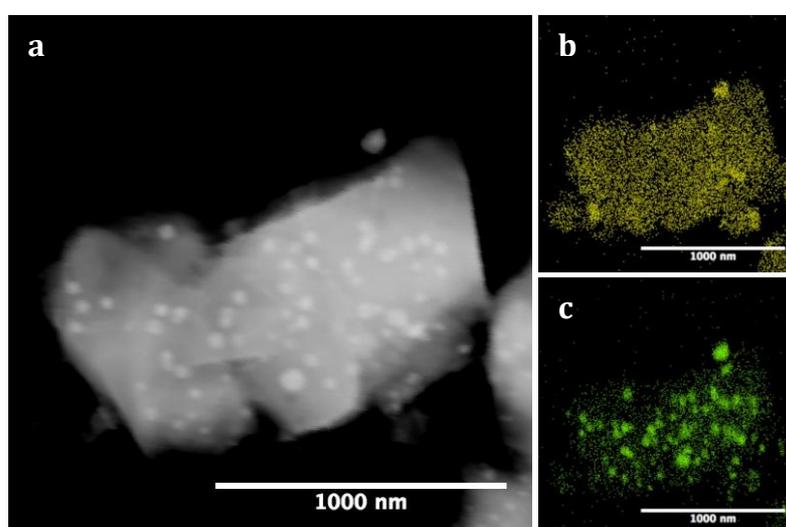
Figure 5: Elemental mapping by TEM of Ni_xP_y/H^+ Y zeolite catalyst prepared in a single-step impregnation (a) Electron image, (b) P distribution, (c) Ni distribution

3.2 Effect of base-treatment

A second series of experiments were conducted using the NH_4^+ Y and $H^+ Y_L$ zeolites base-treated with NaOH (0.38 g g^{-1}) and either low (0.2 g g^{-1}) or high concentrations of TPABr (0.92 g g^{-1}), denoted as mild treatment (MT) and harsh treatment (HT), respectively.

15

The objective of the base-treatment step was to introduce additional mesopores into the supports, thereby producing hierarchical zeolites with the aim of reducing potential mass transfer limitations through the resulting catalysts. Once again, the quinoline conversion activity was tested for both the bare hierarchical zeolites, and the supported nickel phosphide materials.

3.2.1 Bare hierarchical zeolites

Following base treatment, both the NH_4^+ Y and H^+ Y_L zeolites experienced a dramatic decrease in quinoline conversion activity, with product distributions similar to those achieved in the blank reaction (Figure 7). This confirms our previous hypothesis suggesting that the catalytic activity of the blank zeolites is predominantly related to cracking reaction over the Brønsted acid sites, which are neutralised during base treatment. Interestingly, base treatment had opposite effects on the surface areas and unit cell parameters of the two materials (Table 1): for NH_4^+ Y, the surface area increased from $765\,m^2\,g^{-1}$ to $898\,m^2\,g^{-1}$ and the cell parameter reduced from $24.61\,\text{Å}$ to $24.52\,\text{Å}$ following mild base treatment, whereas for H^+ Y_L, the surface area reduced from $919\,m^2\,g^{-1}$ to $684\,m^2\,g^{-1}$ and the cell parameter increased from $24.23\,\text{Å}$ to $24.33\,\text{Å}$. These trends can be explained by the significant increase of the Na^+/Al ratios following base treatment, related to the ion exchange of the NH_4^+ and H^+ counterions with Na^+. As the larger NH_4^+ ions are replaced with the smaller Na^+ ions, the surface areas increase for the NH_4^+ Y zeolites, whereas the H^+ ions are smaller than Na^+, resulting in a surface area decrease following ion exchange.

Base treatment also had a very different effect on the Si/Al ratios (from SEM-EDX analysis) in the two zeolites. In the case of the NH_4^+ Y zeolite, the ratio remained approximately constant around 2.5, but decreased significantly from 17.9 ($\pm\,1.4$) to 11.5 ($\pm\,0.2$) for the H^+ Y_L zeolite after harsh base treatment. This suggests that the base-treatment preferentially attacks the Si-Si bonds, whereas the Si-Al bonds are more stable, [49] making the base treatment step less effective. Consequently, further analysis was restricted to the H^+ Y_L zeolites only. SEM analysis showed that the untreated samples displayed smooth surfaces, whereas additional surface porosity became apparent for the material treated with a TPABr concentration of $0.92\,g\,g^{-1}$ (supplementary information). Further evidence for the emergence of mesopores in the zeolite structure was obtained from nitrogen adsorption measurements. Fitting the data against both the BJH (suited to meso/small macropores) and NLDFT models revealed the emergence of additional porosity within the 2 nm to 12 nm range for the material exposed to harsh base treatment (Figure 8).

Combined with the conversion data it is clear that base treatment and the emergence of porosity within the mesopore range has no beneficial impact on the conversion of quinoline over the bare zeolites. This suggests that the treatment process reduces the number of active catalytic sites on the zeolite surface, counteracting any potential effect of improved mass transfer through the zeolite.

3.2.2 Ni-P catalysts on hierarchical zeolite supports

To preserve the structure of the base-treated zeolites and based on the results from the previous study using the zeolites containing different counterions, nickel phosphide catalysts supported on the base-treated zeolites were prepared using the single-step impregnation method only. For the NH_4^+ Y supported catalysts, a clear reduction in overall quinoline conversion and 5678THQ selectivity was observed for the catalysts on the base-treated supports (Figure 7b). This trend can be explained using the corresponding XRD powder diffraction patterns which display a shift from a pure Ni_2P phase formed on the untreated zeolite towards $Ni_2P/Ni_{12}P_5$ phases for the base treated supports (Figure 9a). This leads to a decrease on the overall quinoline conversion due to the lower activity of the $Ni_{12}P_5$ species compared to Ni_2P as discussed above. In contrast, the overall quinoline conversion over the H^+ Y_L catalysts is less affected by base treatment of the support, whilst the selectivity towards the partial hydrogenation products 1234THQ and 5678THQ increases marginally. In this case, a pure Ni_2P phase is observed on the XRD powder diffraction patterns, potentially due to the lower Al content, resulting in reduced Al-P interaction (Figure 9b).

STEM-EDX analysis of the base treated NH_4^+ Y and H^+ Y zeolite supported catalysts shows a much lower phosphorus dispersion across the H^+ Y_L zeolite surface than over the NH_4^+ Y surface, consistent with the discussion above (Figures 10 and 11). Nevertheless, the catalyst supported on base-treated hierarchical NH_4^+ Y contains a higher Ni/P ratio than its untreated counterpart, suggesting that the base treatment decreases the amount of surface bound P, despite the same Si/Al ratio (Table 3). Moreover, the crystallite sizes of the nickel species, as determined by Scherrer equation, show a clear increase after base treatment of the NH_4^+ Y zeolite support, which is also expected to reduce the concentration of the square pyramidal edge sites responsible for the hydrogenation activity as discussed above. In contrast, the crystallite sizes of the H^+ Y_L zeolite supported catalysts are approximately constant regardless of base treatment.

A potential explanation for the shift over the NH_4^+ Y supported catalysts is the ion exchange of NH_4^+ with Na^+ during the base-treatment process and/or the high Na content after base

treatment (Table 1). This observation is consistent with the presence of the mixed $Ni_2P/Ni_{12}P_5$ phase for the Na^+ Y supported catalysts in the previous section.

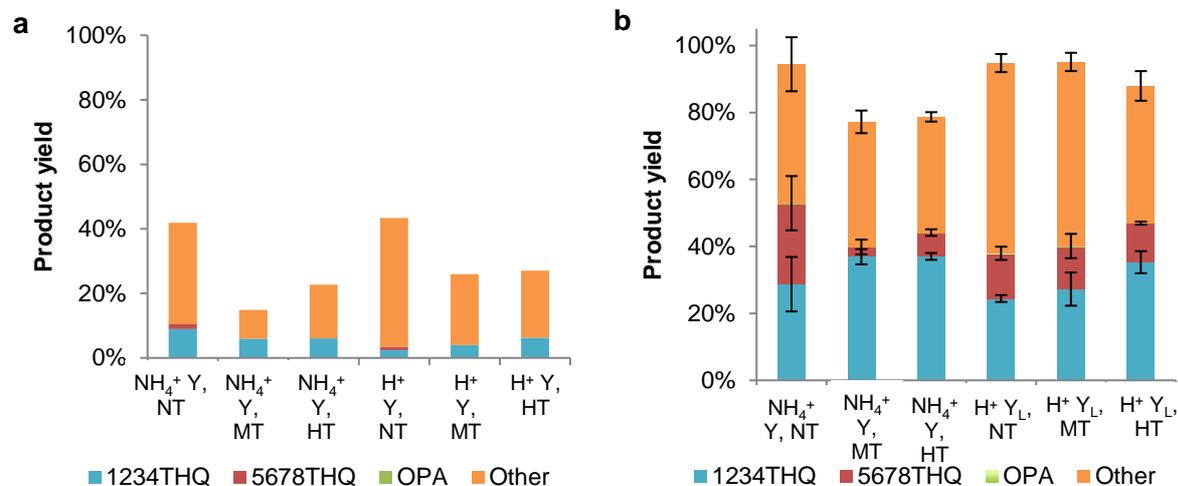**Figure 6: Effect of base treatment on the quinoline conversion over (a) bare NH_4^+ Y and H^+ Y zeolites and (b) supported Ni_xP_y/NH_4^+ Y and Ni_xP_y/H^+ Y base-treated zeolites. (NT: no treatment, MT: mild treatment, HT: harsh treatment)**
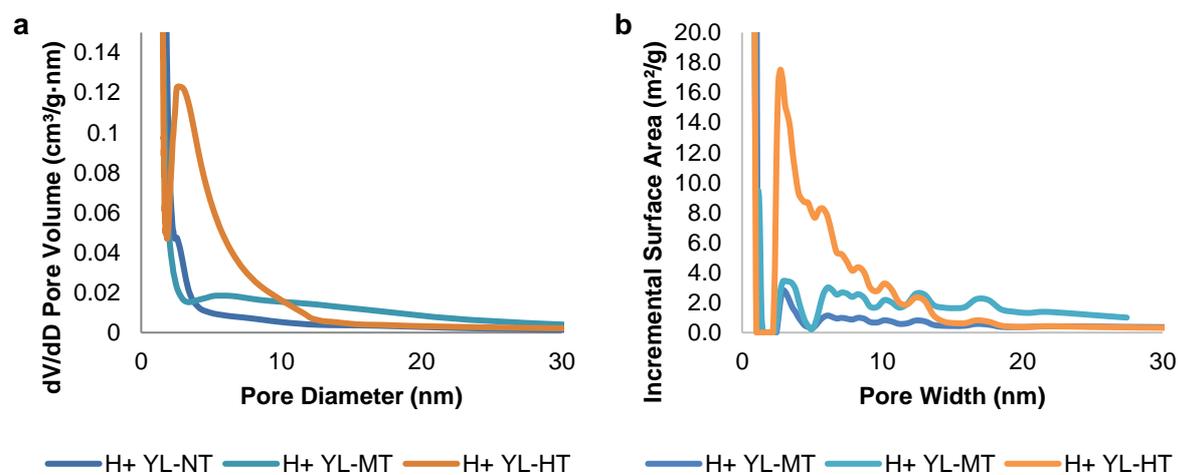

Figure 8: Estimation of pore size distribution for base treated H^+ Y_L zeolite. (a) BJH adsorption with Kruk-Jaroniec-Sayari correction model applied, (b) NLDFT analysis with Kruk-Jaroniec-Sayari correction model applied
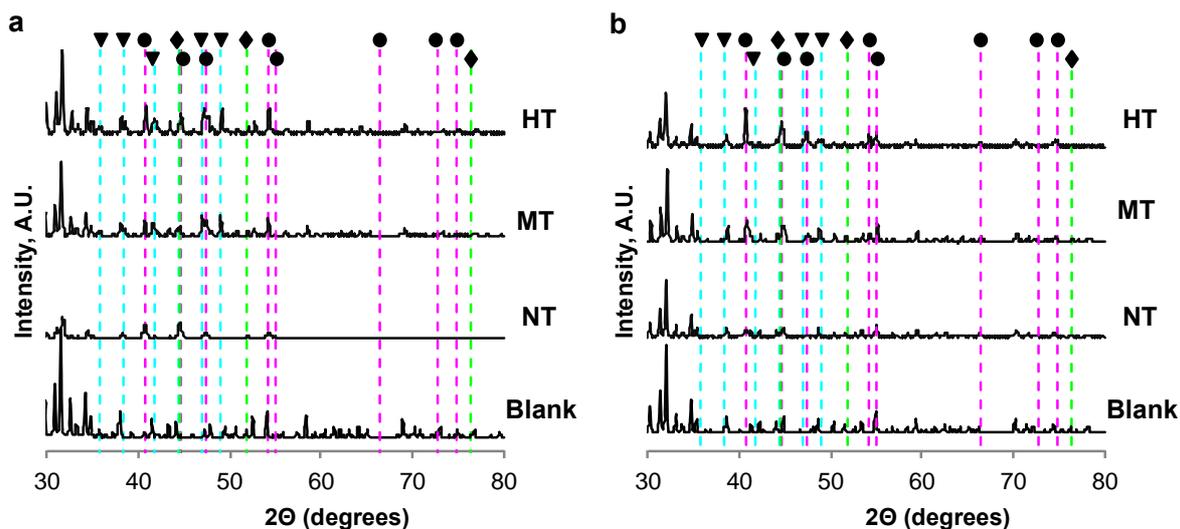
Figure 9: XRD patterns of catalysts Ni_xP_y supported on (a) NH_4^+ Y zeolite and (b) H^+ Y_L zeolite. Blank: commercial zeolite, NT: untreated, MT: mild base treatment, HT: harsh base treatment. ($\blacklozenge$ = Ni^0, $\bullet$ = Ni_2P, $\blacktriangledown$ = $Ni_{12}P_5$)

Table 3: Physical properties of nickel phosphide catalysts supported on NH_4^+ Y zeolite - effect of base treatment

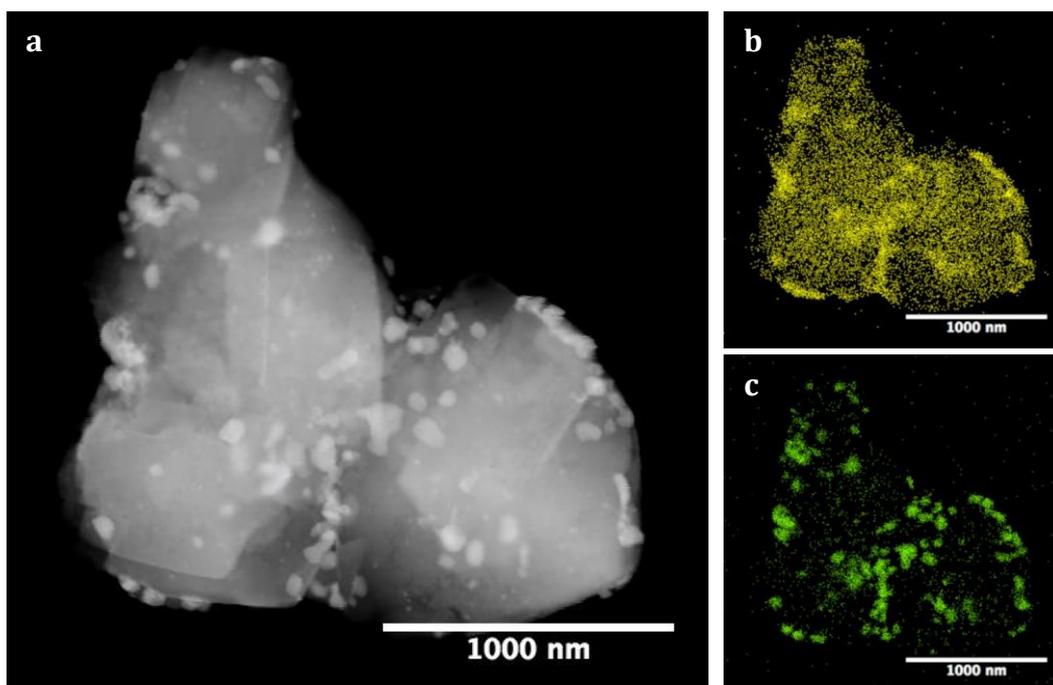| Support	SEM-EDX analysis		BET Surface area, m^2 g^{-1}	FWHM of [1 1 1] zeolite peak, degrees	Ni phase	Ni-P particle size, nm
	Ni loading / % wt.	Ni/P ratio				
NH_4^+ Y	2.6[x]	0.23[x]	226	0.246	Ni_2P	18.08*
NH_4^+ Y-MT	4.0	0.48	328	0.197	$Ni_2P/Ni_{12}P_5$	39.12*
NH_4^+ Y-HT	3.8	0.50	330	0.246	$Ni_2P/Ni_{12}P_5$	35.74*
H^+ Y_L	5.0	0.76	597	0.197	Ni_2P	30.11*
H^+ Y_L-MT	3.2	0.60	535	0.246	Ni_2P	26.21*
H^+ Y_L-HT	3.3	0.63	426	0.197	Ni_2P	28.77*

Figure 7: Elemental mapping by TEM of Ni$_x$P$_y$/NH$_4^+$ Y-HT zeolite catalyst after harsh base treatment prepared in a single-step impregnation (a) Electron image, (b) P distribution, (c) Ni distribution
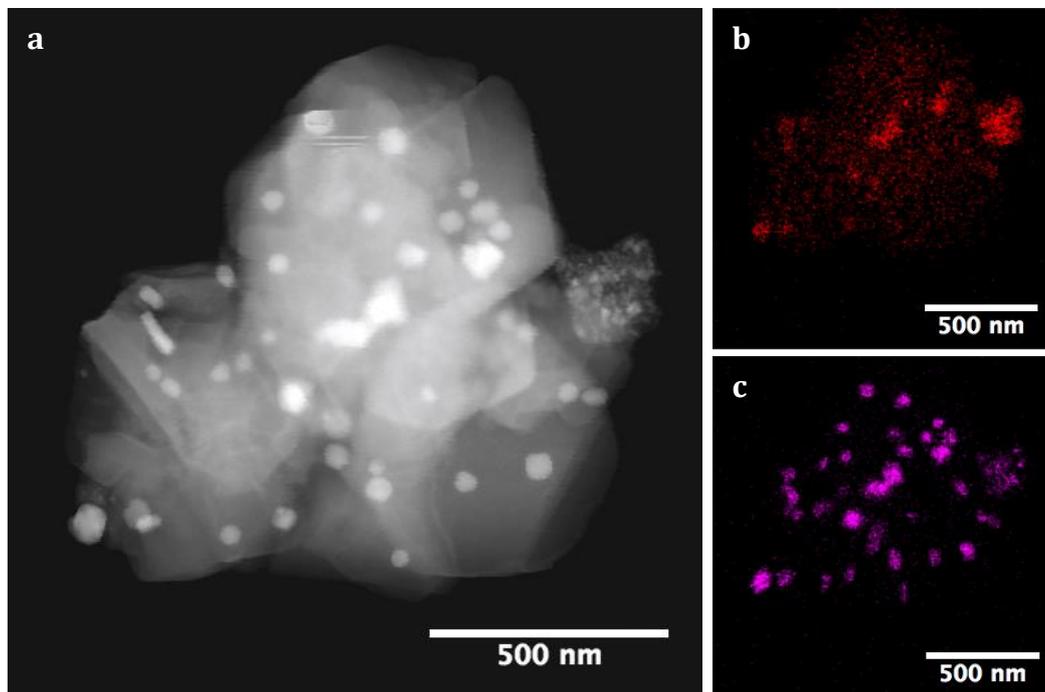

Figure 8: Elemental mapping by TEM of Ni$_x$P$_y$/H$^+$ Y$_L$-HT zeolite catalyst after harsh base treatment prepared in a single-step impregnation (a) Electron image, (b) P distribution, (c) Ni distribution

3.3 Comparison with quinoline conversion over baseline catalysts

In order to compare the activity of the Ni_xP_y supported catalysts with conventional metal and transition metal catalysts, commercial 5 wt.% Pd/C, $NiCoMo/Al_2O_3$ (1.6 wt.% Ni, 1.6 wt.% Co, 15 wt.% Mo) and $NiMo/CeO_2$ (6.0 wt.% NiO, 30 wt.% MoO_3, 64 wt.% CeO_2) were tested for the hydrodenitrogenation reaction under the same experimental conditions (Figure 12). Generally, the levels of conversion of quinoline were comparable to those achieved by the supported Ni_xP_y/Y-zeolite catalysts. The differences in the product distribution are obviously related to the nature of the active sites in each system. The most relevant case is the product distribution achieved with the 5 wt.% Pd/C, where a very small 1234THQ concentration is obtained, suggesting that palladium greatly favours the hydrogenation of the aromatic ring adjacent to the nitrogen heterocycle in a selective manner. On the other hand, the transition metal catalysts seem to favour the hydrogenation of the nitrogen-containing aromatic ring.

These studies indicate that for upgrading of bio-oils containing low sulphur content, the supported Ni_xP_y/Y-zeolite catalysts could indeed be a feasible sustainable alternative for the upgrading of bio-oils.
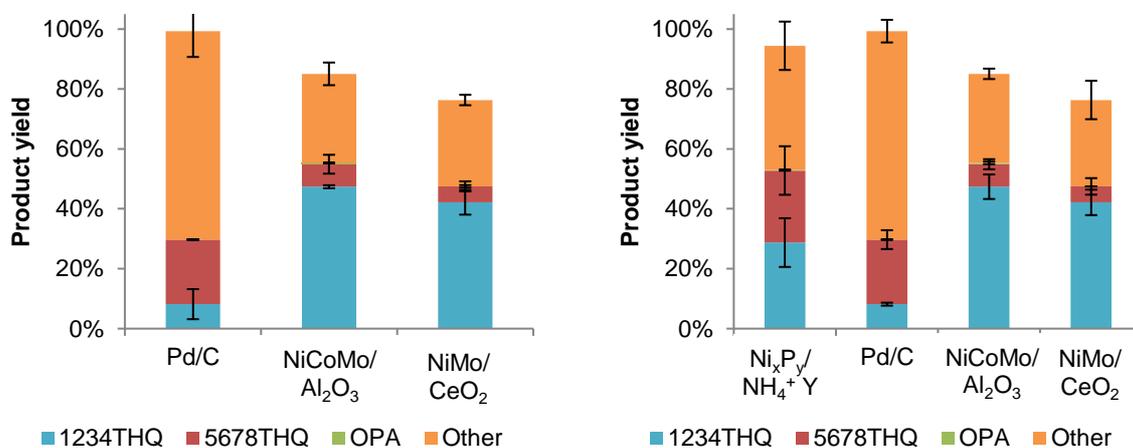

Figure 9: Quinoline conversion over conventional metal and transition metal catalysts, compared to most active nickel phosphide catalyst (Ni_xP_y on NH_4^+ Y, prepared by single step impregnation)

4 Conclusions

This study presents zeolite Y supported nickel phosphides as alternative catalysts for the hydrodenitrogenation of heterocycles typically found in crude bio-oils, displaying comparable quinoline denitrogenation activities to noble metal and transition metal catalysts. Bare zeolite supports on their own caused a distinct increase in quinoline conversion compared to a blank reaction, but had no beneficial impact on the initial hydrogenation step. Their activity was independent of the choice of counterion (NH_4^+, H^+, Na^+ and K^+), their Si/Al ratio and their surface area. A notable exception is the Ni^{2+} Y zeolite, which yielded higher amounts of the partial hydrogenation products 1234THQ as well as 5678THQ together with a significant increase in overall conversion. However, this catalyst presents low selectivity towards the direct quinoline denitrogenation pathway. Base treatment of NH_4^+ Y and H^+ Y with NaOH and TPABr was more effective for the low aluminium zeolite (H^+ Y_L), due to the selective dissolution of silicon, resulting in the formation of mesopores in the 2 nm to 12 nm range. However this treatment had no beneficial impact on the quinoline conversion activity of the bare zeolites, indicating that mass transport may not be a major limitation in the conversion of the quinoline model compound.

The impregnation of the different Y-zeolite supports with Ni and P yielded catalysts with high quinoline conversion activities and high yields of the partial hydrogenation products 1234THQ and 5678THQ. Both the zeolite counterion and the impregnation method (single or two-step impregnation) had a noticeable impact on the catalyst activity, and this was related to the predominant Ni_xP_y species formed in the material. $Ni_{12}P_5$ was the least active, metallic Ni favoured the hydrogenation of the nitrogen-containing aromatic ring as the first reaction step, whilst Ni_2P allowed both the initial hydrogenation of the nitrogen-containing aromatic ring and the initial saturation of the aromatic rings adjacent to the nitrogen heterocycle, leading to a higher final yield of fully hydrodenitrogenated products. Decreasing nanoparticle sizes were also found to give increased yields of 5678THQ, consistent with the higher hydrogenation activities previously proposed for the square pyramidal sites, which are more predominant in smaller particles.

These studies indicate the enormous potential of Y-zeolite supported nickel phosphides as a new class of catalysts suitable for the catalytic upgrading of crude bio-oils to value products. Nonetheless, it is obvious that our initial results will need to be verified using actual algal bio-oil. Furthermore, while the stability of nickel phosphide catalysts is well known [25,29,30] cycling studies should be conducted to determine the reusability of these catalysts in such applications.
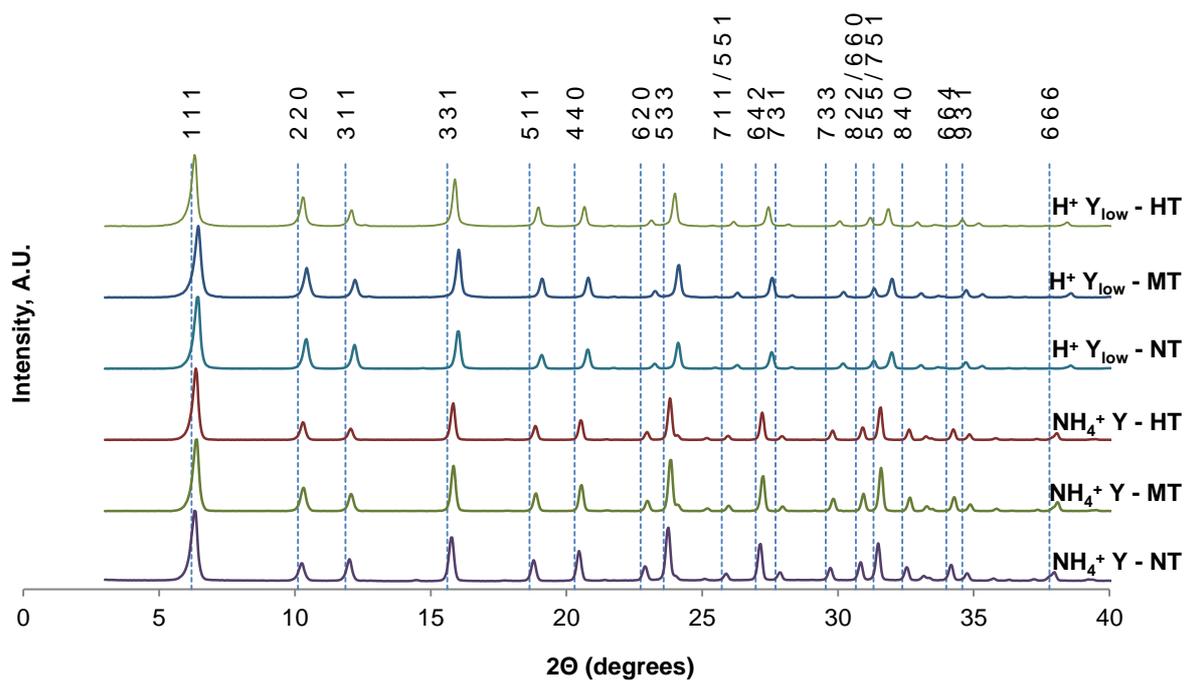
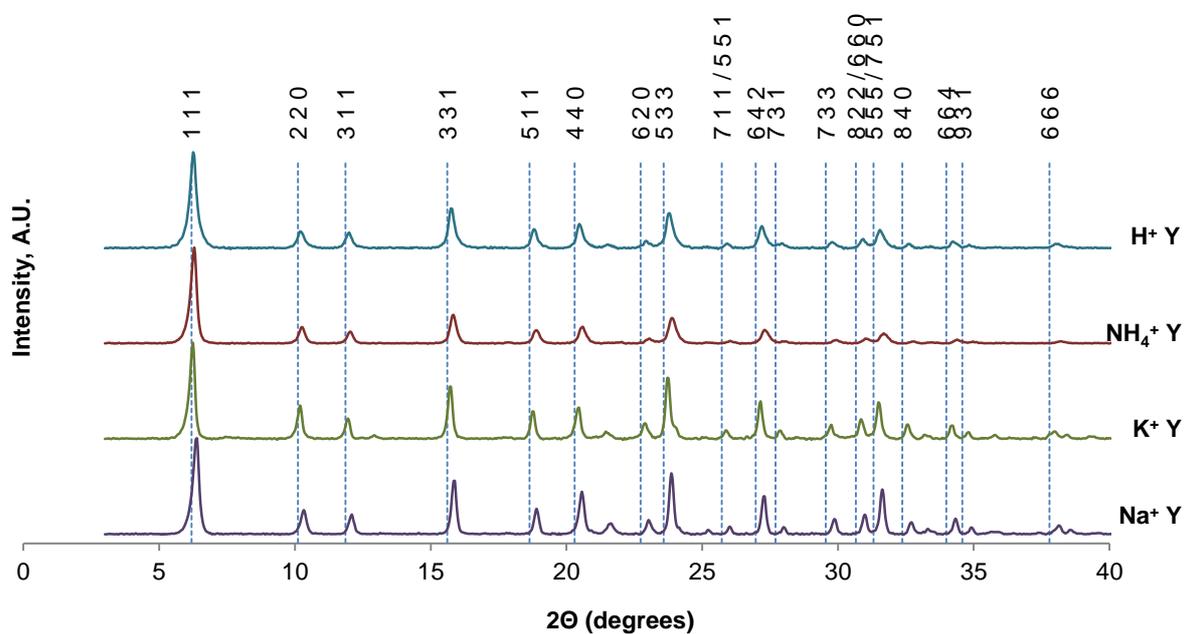# 5 Supplementary information

5.1 X-Ray powder diffraction patterns
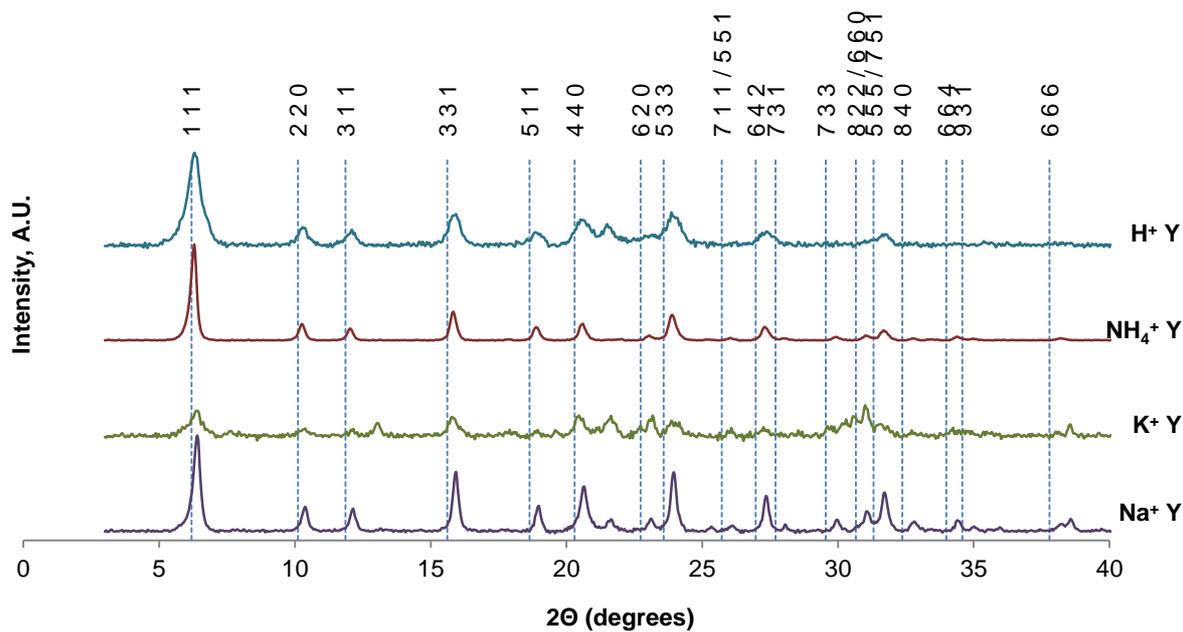
5.1.1 Ion-exchanged zeolites
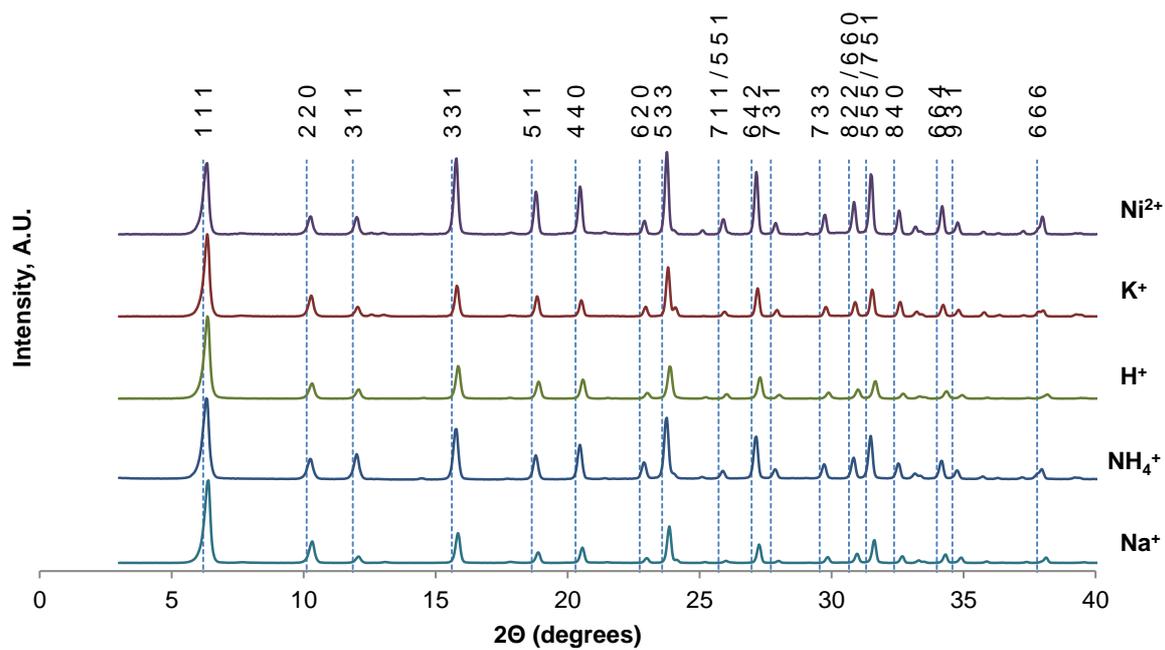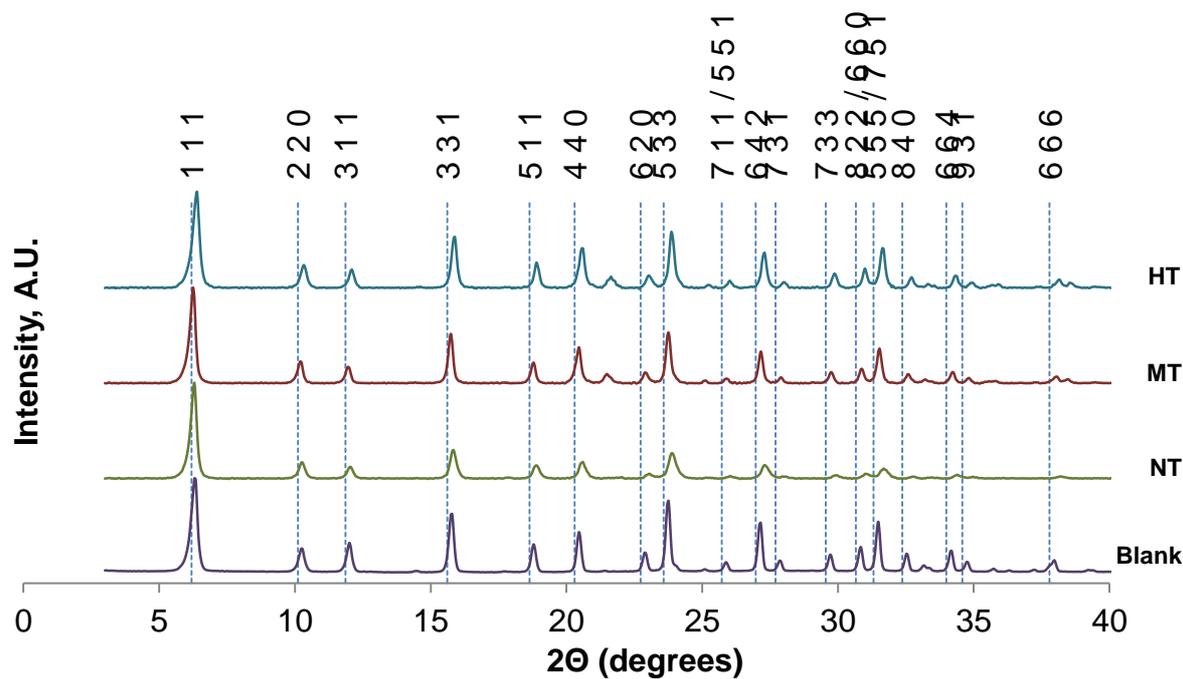
5.1.2 Base-treated zeolites

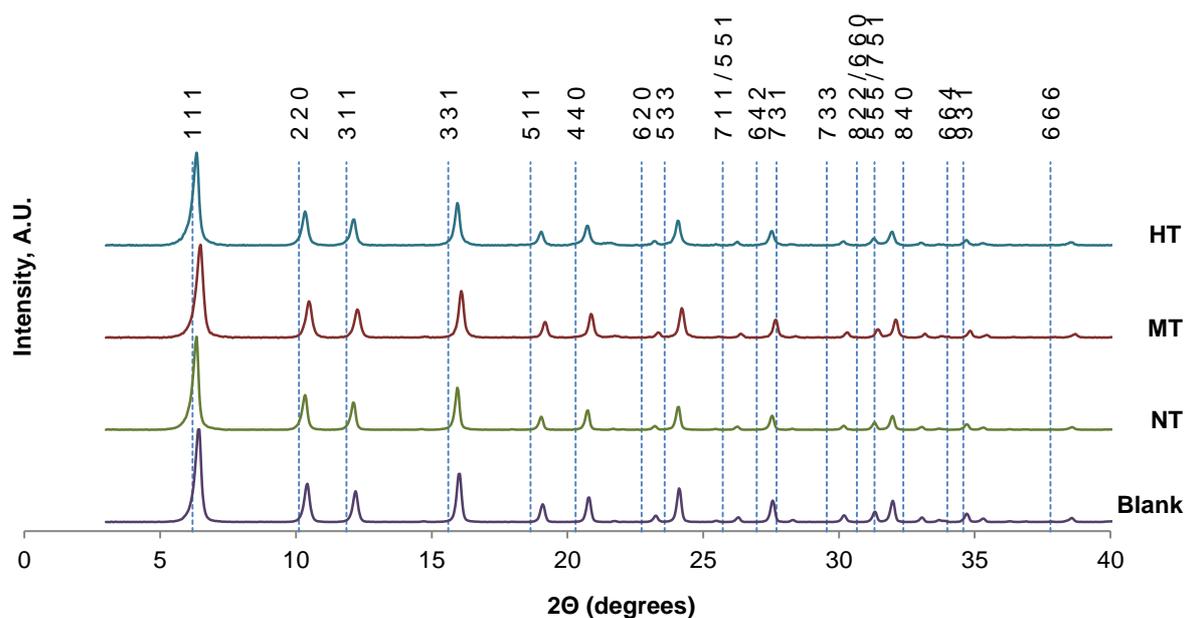## 5.1.3 Ni-P catalysts prepared by single step impregnation

5.1.4 Ni-P catalysts prepared by two-step impregnation

5.1.5 Ni-P catalysts supported on base-treated NH_4^+ Y zeolite (single-step impregnation)

5.1.6 Ni-P catalysts supported on base-treated $H^+ Y_L$ zeolite (single-step impregnation)

Intensity, A.U.

111 · 220 · 311 · 331 · 511 · 440 · 620 533 · 711/551 · 642 731 · 733 822/660 555/751 840 · 664 931 · 666

HT

MT

NT

Blank

2Θ (degrees)

5.2 Conversion product of quinoline over Ni²⁺ Y zeolite. Theoretical peaks are listed on the left, whereas the actual peaks are assigned to each product and missing peaks are denoted by an X.

Theoretical peaks	1234THQ	5678THQ	OPA	tDHQ	cDHQ	PCH	PB
157.28		x					
146.73		x					
144.80	144.66						
144.14			x				
136.60		x					
132.12		x					
129.48			129.40				
129.40	129.40						
126.83			x				
126.65	126.62						
126.64			126.62				
121.26	121.28						
120.80		120.93					
118.62			x				
116.77	116.88						
115.49			x				
114.12	114.08						
53.28				x			
50.49					x		
47.31				x			
45.52					x		
43.85				x			
42.52				x			
41.93	41.92						
40.04						x	
37.56						x	
36.54					x		
34.74					x		
34.43				x			
33.64				x			
33.58						x	
33.33			x				
32.52		x					
30.57				x			
30.11					x		
28.86					x		
28.73		28.69					

27.00	26.91						
26.89						26.91	
26.85					x		
26.61						x	
26.53				x			
26.31				x			
25.05					x		
23.09		x					
22.90					x		
22.71		x					
22.17	22.16						
21.86							
20.04						x	
14.46						14.36	
14.13			x				

5.3   **SEM analysis of base treated H$^+$ Y$_L$ zeolite samples. (a) untreated zeolite, (b) and (c) zeolite following harsh chemical treatment, displaying small surface defects**
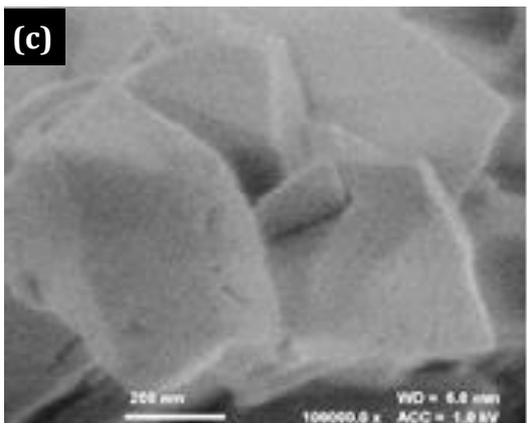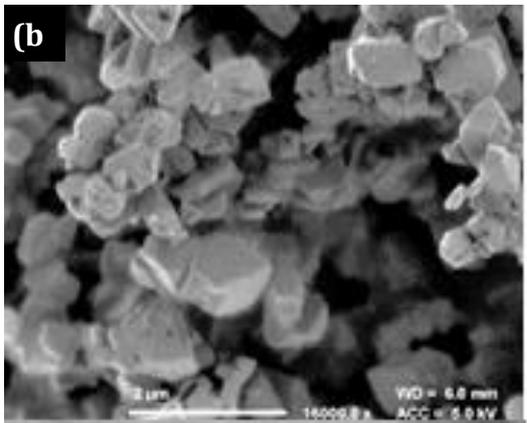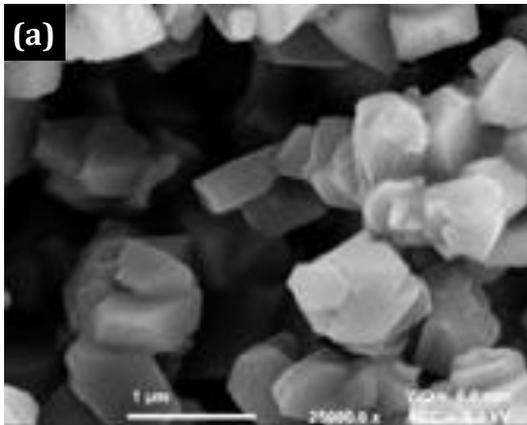
6 References

- 1.   Chiaramonti, D., et al., *Review and experimental study on pyrolysis and hydrothermal liquefaction of microalgae for biofuel production.* Applied Energy, 2017. **185, Part 2**: p. 963-972.
- 2.   Raikova, S., et al., *Assessing hydrothermal liquefaction for the production of bio-oil and enhanced metal recovery from microalgae cultivated on acid mine drainage.* Fuel Processing Technology, 2016. **142**: p. 219-227.
- 3.   Wagner, J., et al., *Co-production of bio-oil and propylene through the hydrothermal liquefaction of polyhydroxybutyrate producing cyanobacteria.* Bioresour Technol, 2016. **207**: p. 166-74.
- 4.   Bridgwater, A.V., *Review of fast pyrolysis of biomass and product upgrading.* Biomass and bioenergy, 2012. **38**: p. 68-94.
- 5.   Chisti, Y., *Constraints to commercialization of algal fuels.* J Biotechnol, 2013. **167**(3): p. 201-14.
- 6.   Raikova, S., et al., *Towards an Aviation Fuel Through the Hydrothermal Liquefaction of Algae*, in *Biofuels for Aviation - Feedstocks, Technology and Implementation*, C.J. Chuck, Editor. 2016, Elsevier: London.
- 7.   Jechura, J. *Refinery Feedstocks & Products - Properties & Specifications.* 2016 29/08/2016 30 August 2016]; Available from: http://inside.mines.edu/~jjechura/Refining/02_Feedstocks_&_Products.pdf.
- 8.   Valdez, P.J., J.G. Dickinson, and P.E. Savage, *Characterization of Product Fractions from Hydrothermal Liquefaction ofNannochloropsissp. and the Influence of Solvents.* Energy & Fuels, 2011. **25**(7): p. 3235-3243.
- 9.   Chakraborty, M., et al., *Concomitant extraction of bio-oil and value added polysaccharides from Chlorella sorokiniana using a unique sequential hydrothermal extraction technology.* Fuel, 2012. **95**: p. 63-70.
- 10.   Jazrawi, C., et al., *Pilot plant testing of continuous hydrothermal liquefaction of microalgae.* Algal Research, 2013. **2**(3): p. 268-277.
- 11.   Yang, C., et al., *Catalytic hydroprocessing of microalgae-derived biofuels: a review.* Green Chem., 2016. **18**(13): p. 3684-3699.
- 12.   López Barreiro, D., et al., *Heterogeneous catalytic upgrading of biocrude oil produced by hydrothermal liquefaction of microalgae: State of the art and own experiments.* Fuel Processing Technology, 2016. **148**: p. 117-127.
- 13.   Zhang, C., et al., *Catalytic upgrading of duckweed biocrude in subcritical water.* Bioresour Technol, 2014. **166**: p. 37-44.
- 14.   Xu, Y., P. Duan, and B. Wang, *Catalytic upgrading of pretreated algal oil with a two-component catalyst mixture in supercritical water.* Algal Research, 2015. **9**: p. 186-193.
- 15.   Duan, P. and P.E. Savage, *Catalytic treatment of crude algal bio-oil in supercritical water: optimization studies.* Energy & Environmental Science, 2011. **4**(4): p. 1447.
- 16.   Duan, P., et al., *Catalytic upgrading of crude algal oil using platinum/gamma alumina in supercritical water.* Fuel, 2013. **109**: p. 225-233.
- 17.   Duan, P. and P.E. Savage, *Upgrading of crude algal bio-oil in supercritical water.* Bioresour Technol, 2011. **102**(2): p. 1899-906.

- 18.   Duan, P. and P.E. Savage, *Catalytic hydrotreatment of crude algal bio-oil in supercritical water.* Applied Catalysis B: Environmental, 2011. **104**(1-2): p. 136-143.
- 19.   Costanzo, W., et al., *Low temperature hydrothermal pretreatment of algae to reduce nitrogen heteroatoms and generate nutrient recycle streams.* Algal Research, 2015. **12**: p. 377-387.
- 20.   Biller, P., et al., *Hydroprocessing of bio-crude from continuous hydrothermal liquefaction of microalgae.* Fuel, 2015. **159**: p. 197-205.
- 21.   Elliott, D.C., et al., *Process development for hydrothermal liquefaction of algae feedstocks in a continuous-flow reactor.* Algal Research, 2013. **2**: p. 445-454.
- 22.   Korányi, T.I., Z. Vít, and J.B. Nagy, *Support and pretreatment effects on the hydrotreating activity of SBA-15 and CMK-5 supported nickel phosphide catalysts.* Catalysis Today, 2008. **130**(1): p. 80-85.
- 23.   Oyama, S.T., et al., *Structural Characterization of Tungsten Phosphide (WP) Hydrotreating Catalysts by X-ray Absorption Spectroscopy and Nuclear Magnetic Resonance Spectroscopy.* The Journal of Physical Chemistry B, 2002. **106**(8): p. 1913-1920.
- 24.   Oyama, S., *Effect of Phosphorus Content in Nickel Phosphide Catalysts Studied by XAFS and Other Techniques.* Journal of Catalysis, 2002. **210**(1): p. 207-217.
- 25.   Lu, M., et al., *Hydrodenitrogenation of Quinoline Catalyzed by MCM-41-Supported Nickel Phosphides.* Energy & Fuels, 2007. **21**(2): p. 554-560.
- 26.   Oyama, S., *Novel catalysts for advanced hydroprocessing: transition metal phosphides.* Journal of Catalysis, 2003. **216**(1-2): p. 343-352.
- 27.   Lee, Y.-K., Y. Shu, and S.T. Oyama, *Active phase of a nickel phosphide (Ni2P) catalyst supported on KUSY zeolite for the hydrodesulfurization of 4,6-DMDBT.* Applied Catalysis A: General, 2007. **322**: p. 191-204.
- 28.   Oyama, S.T., et al., *Transition metal phosphide hydroprocessing catalysts: A review.* Catalysis Today, 2009. **143**(1-2): p. 94-107.
- 29.   Stinner, C., R. Prins, and T. Weber, *Binary and Ternary Transition-Metal Phosphides as HDN Catalysts.* Journal of Catalysis, 2001. **202**(1): p. 187-194.
- 30.   Robinson, W., et al., *Phosphorus promotion of Ni(Co)-containing Mo-free catalysts in quinoline hydrodenitrogenation.* Journal of Catalysis, 1996. **161**(2): p. 539-550.
- 31.   Zhao, H.Y., et al., *Hydrodeoxygenation of guaiacol as model compound for pyrolysis oil on transition metal phosphide hydroprocessing catalysts.* Applied Catalysis A: General, 2011. **391**(1-2): p. 305-310.
- 32.   Koike, N., et al., *Upgrading of pyrolysis bio-oil using nickel phosphide catalysts.* Journal of Catalysis, 2016. **333**: p. 115-126.
- 33.   Kanda, Y., et al., *Preparation and performance of noble metal phosphides supported on silica as new hydrodesulfurization catalysts.* Applied Catalysis A: General, 2010. **386**(1-2): p. 171-178.
- 34.   Infantes-Molina, A., et al., *Ni2P and CoP catalysts prepared from phosphite-type precursors for HDS–HDN competitive reactions.* Applied Catalysis A: General, 2010. **390**(1-2): p. 253-263.
- 35.   Zhang, S., et al., *A general approach to the synthesis of metal phosphide catalysts.* Powder Technology, 2014. **253**: p. 509-513.

- 36. Song, L., S. Zhang, and Q. Wei, *A new route for synthesizing nickel phosphide catalysts with high hydrodesulfurization activity based on sodium dihydrogenphosphite.* Catalysis Communications, 2011. **12**(12): p. 1157-1160.
- 37. Stinner, C., R. Prins, and T. Weber, *Formation, Structure, and HDN Activity of Unsupported Molybdenum Phosphide.* Journal of Catalysis, 2000. **191**(2): p. 438-444.
- 38. Clark, P., *Alumina-supported molybdenum phosphide hydroprocessing catalysts.* Journal of Catalysis, 2003. **218**(1): p. 78-87.
- 39. Song, H., et al., *A novel synthesis of Ni2P/MCM-41 catalysts by reducing a precursor of ammonium hypophosphite and nickel chloride at low temperature.* Applied Catalysis A: General, 2013. **462-463**: p. 247-255.
- 40. Kim, Y.-S., G.-N. Yun, and Y.-K. Lee, *Novel Ni2P/zeolite catalysts for naphthalene hydrocracking to BTX.* Catalysis Communications, 2014. **45**: p. 133-138.
- 41. Suresh, C., et al., *Mo–Ni/Al-SBA-15 (Sulfide) Catalysts for Hydrodenitrogenation: Effect of Si/Al Ratio on Catalytic Activity.* ACS Catalysis, 2012. **2**(1): p. 127-134.
- 42. Qu, L. and R. Prins, *Different active sites in hydrodenitrogenation as determined by the influence of the support and fluorination.* Applied Catalysis A: General, 2003. **250**(1): p. 105-115.
- 43. Prins, R. and M.E. Bussell, *Metal Phosphides: Preparation, Characterization and Catalytic Reactivity.* Catalysis Letters, 2012. **142**(12): p. 1413-1436.
- 44. Guan, Q., et al., *Hydrodeoxygenation of methyl palmitate over MCM-41 supported nickel phosphide catalysts.* Catalysis Today, 2016. **259**: p. 467-473.
- 45. Sawada, A., et al., *Rhodium phosphide catalyst for hydrodesulfurization: Low temperature synthesis by sodium addition.* Catalysis Communications, 2014. **56**: p. 60-64.
- 46. Sawhill, S., et al., *Thiophene hydrodesulfurization over nickel phosphide catalysts: effect of the precursor composition and support.* Journal of Catalysis, 2005. **231**(2): p. 300-313.
- 47. Holm, M.S., et al., *Catalysis with hierarchical zeolites.* Catalysis Today, 2011. **168**(1): p. 3-16.
- 48. van Donk, S., et al., *Generation, Characterization, and Impact of Mesopores in Zeolite Catalysts.* Catalysis Reviews, 2003. **45**(2): p. 297-319.
- 49. Ogura, M., et al., *Alkali-treatment technique — new method for modification of structural and acid-catalytic properties of ZSM-5 zeolites.* Applied Catalysis A: General, 2001. **219**(1-2): p. 33-43.
- 50. Wang, W., et al., *Influences of calcination and reduction methods on the preparation of Ni2P/SiO2 and its hydrodenitrogenation performance.* Applied Catalysis A: General, 2016. **509**: p. 45-51.
- 51. Holland, T.J.B., *Unit Cell Refinement from Powder Diffraction Data: The Use of Regression Diagnostics.* Mineralogical Magazine, 1997. **61**(404): p. 65-77.
- 52. Treacy, M.M.J. and J.B. Higgins, *Collection of Simulated XRD Powder Patterns for Zeolites*. 4th ed, ed.
Structure Commission of the International Zeolite Association. 2001, Amsterdam: Elsevier.
- 53. Jena, U., K.C. Das, and J.R. Kastner, *Effect of operating conditions of thermochemical liquefaction on biocrude production from Spirulina platensis.* Bioresour Technol, 2011. **102**(10): p. 6221-9.

- 54.   Laine, R.M., *Modeling heterogeneous catalysts with homogeneous catalysts: modeling the hydrodenitrogenation reaction.* Journal of Molecular Catalysis, 1983. **21**(1-3): p. 119-132.
- 55.   Perot, G., *The reactions involved in hydrodenitrogenation.* Catalysis Today, 1991. **10**(4): p. 447-472.
- 56.   Jokuty, P.L. and M.R. Gray, *Nitrogen bases resistant to hydrodenitrogenation: evidence against using quinoline as a model compound.* Industrial & Engineering Chemistry Research, 1992. **31**(6): p. 1445-1449.
- 57.   Collins, D.J., E.C. Lloyd, and R. Miranda, *Side reactions in quinoline hydrodenitrogenation.* Applied Catalysis, 1988. **41**: p. 81-88.
- 58.   Yan, K., et al., *Effect of preparation method on Ni2P/SiO2 catalytic activity for NaBH4 methanolysis and phenol hydrodeoxygenation.* International Journal of Hydrogen Energy, 2015. **40**(46): p. 16137-16146.
- 59.   Davis, R., A. Aden, and P.T. Pienkos, *Techno-economic analysis of autotrophic microalgae for fuel production.* Applied Energy, 2011. **88**(10): p. 3524-3531.
- 60.   Chen, J., et al., *Deoxygenation of methyl laurate as a model compound to hydrocarbons on transition metal phosphide catalysts.* Applied Catalysis B: Environmental, 2014. **144**: p. 870-884.
- 61.   Zhang, L., et al., *Ni2P clusters on zeolite nanosheet assemblies with high activity and good stability in the hydrodesulfurization of 4,6-dimethyldibenzothiophene.* Journal of Catalysis, 2016. **338**: p. 210-221.